Journal of Translational Medicine

RESEARCH

Open Access

A novel bispecific affitoxin simultaneously targeting E7 of HPV16/18 types: superior anti-tumor activity and EMT reversal in HPV-driven cervical cancer therapy

Kairong Wan[1], Lijun Yu[1], Sicong Feng[1], Zhenyun Xie[2], Yanheng Li[1], Xisha Jing[1], Junze Wu[1], Lifang Zhang[1*] and Wenshu Li[1*]

Abstract

Background Sustained infection with high-risk HPV of the 16 and 18 types is accounted for nearly 75% of cervical cancer (CC), but now there is an absence of agents aimed at eradicating HPV infections. Notwithstanding, affibody-based affitoxins may represent a breakthrough in tumor-targeted therapy. Our previous work has constructed a bispecific affibody simultaneously targeting the early oncogenic proteins E7 of HPV16 and 18 types (named as $Z_{HPV16\text{-}18E7}$). In the present study, Granzyme B (GrB, cytotoxic effector) was introduced to construct three bispecific affitoxins for the enhanced therapy against HPV-infected CC cells.

Methods Three forms of the affitoxin constructs (GrB-$Z_{HPV16\text{-}18E7}$, $Z_{HPV16E7}$-GrB-$Z_{HPV18E7}$, and $Z_{HPV16\text{-}18E7}$-GrB) were designed and prepared, and their binding to the target protein and cells were confirmed by SPR analysis and a confocal immunofluorescence assay. The inhibition of cell viability by a CellTiter-Lumi™ luminescence assay, the induction of apoptosis by a fluorometric TUNEL method, and the reversal of EMT by wound healing and transwell assays, for the affitoxins against the target cells were evaluated. The in vivo inhibition in tumor-bearing mice along with the acute toxicity, pharmacokinetics, and stability of the affitoxins were tested.

Results Two bispecific affitoxins of $Z_{HPV16E7}$-GrB-$Z_{HPV18E7}$ and $Z_{HPV16\text{-}18E7}$-GrB were successfully prepared. They can bind to the target protein and cells, inhibited cell viability as well. Compared to the bispecific affibody (without GrB), the bispecific affitoxins induced a more pronounced apoptosis characterized by the release of active caspase-3 and may inhibit cell migration by reversing the epithelial-mesenchymal transition (EMT) pathway. In vivo, the bispecific affitoxin exhibited significant tumor-targeting accumulation in tumor-bearing mice. Compared to the bispecific affibody, the bispecific affitoxin showed a more significant inhibition of the growth of the xenograft tumor in mice, with no acute toxic reactions and a certain degree of stability.

*Correspondence:
Lifang Zhang
lifangzhangwz@126.com
Wenshu Li
lws161@wmu.edu.cn

Full list of author information is available at the end of the article

Conclusions This work has developed a bispecific affitoxin that simultaneously targets HPV16- and HPV18-type CC cells, with a significant dual-functional advantage, combining the targeted inhibitory of the affibody with the cytotoxicity of the toxin molecule. Our research offers a novel design and approach for targeted therapy in HPV-driven cervical cancer.

Keywords HPV16/18, Bispecific affitoxin, Cervical cancer cells, Targeted therapy

Introduction

High-risk human papillomavirus (HR-HPV) persistent infection is responsible for more than 99% of cervical cancer (CC) cases, with HPV16 and 18 types accounting for nearly 75% [1, 2]. CC ranks among the top ten newly diagnosed cancers in China and is increasingly affecting younger populations. Current standard treatments include surgery, radiotherapy, and cisplatin-based chemotherapy, often supplemented with targeted therapy [3]. Given the toxic side effects of radiotherapy and chemotherapy, the issue of drug resistance in targeted therapies, and the lack of targeted therapies specifically against HPV pathogens, there is an urgent need to develop novel targeted treatment agents aimed at eradicating HPV infections.

Antibody–drug conjugates (ADCs) represent a new class of cancer therapeutics that combine the specificity of antibodies with the therapeutic efficacy of drugs. An ADC consists of two components: an antibody that specifically recognizes and binds to target cell surface antigens, and a therapeutic agent (also called cytotoxic payload or warhead) attached to the antibody, thus, improving tumor targeting and anti-tumor potency not achievable with traditional drugs [4–7]. ADCs selectively target tumor cells, significantly reducing side effects compared to traditional chemotherapy, and they demonstrate superior therapeutic efficacy by directly acting on tumor cells. Several ADCs have been clinically applied with promising results, such as trastuzumab-metaxine conjugate (Kadcyl) for breast cancer [8], and brentuximab vedotin (Adcetris) for lymphoma, which consists of a monoclonal antibody targeting CD30 linked to the microtubule-disrupting agent MMAE (Monomethyl Auristatin E) [9, 10]. Notably, Enhertu (trastuzumab deruxtecan, T-DXd) for advanced breast cancer, a conjugation of anti-HER2 (human epidermal growth factor receptor 2) antibody and cytotoxic topoisomerase I inhibitor, was approved in China in 2023 and showed sustained anti-tumor activity, marking a significant breakthrough in ADC drug development [11].

The design of ADCs requires careful selection of both the targeting recognition molecule (antibody or antibody fragment) and the effector molecule (chemotherapy drug or toxin). Monoclonal antibodies are the most commonly used targeting agents but may elicit complement activation and immunogenicity. Toxin molecules, often derived from bacteria or plants, also present immunogenic concerns. Affibody, a small specific binding molecules (approximately 6.5 kDa) selected by affinity screening from a phage library that recognize target proteins, is similar to antibody Fab fragment and enter cells via a caveolin-dependent endocytosis pathway mediated by dynamin, providing a significant cellular uptake advantage over monoclonal antibodies [12, 13], and after conjugation with effector molecules, its anti-tumour activity can be accomplished much more efficiently. Granzyme B (GrB), a potent pro-apoptotic member of the granzyme family released by immune effector cells, induces apoptosis in target cells via caspase activation. As a human-derived cytotoxic effector molecule, GrB does not trigger hypersensitivity reactions or increase metabolic burden, making it an ideal candidate for targeted payload toxin molecules [14–16].

One of the characteristics of HPV-associated malignancy is marked by the sustained expression of oncogenic protein E7 during carcinoma developing and maintaining [17–20]. If suppressing E7, the proliferation of HPV-infected tumor cells will be almost stagnant and followed with apoptosis [21–23]. Metastasis and recurrence in the clinical treatment of CC are real thorny issues, and EMT (epithelial to mesenchymal transition) is an important mechanism for tumor progression, invasion, and metastasis, including HPV-associated malignancy which has found that HPV16E7 can induce EMT in CC cells [24–27]. HPV E7 serves as an indicator of HPV oncogenic activity and a predictor of cervical epithelial cell transformation progression, making it an ideal target for diagnostic or therapeutic approaches. However, therapeutic vaccines targeting HPV E7 have only reached Phase I clinical trials, and while effective anti-HPV immunity has been generated, the outcomes regarding lesion regression and HPV clearance remain unsatisfactory [28]. Designing agents targeting HPV E7 to block the oncogenic pathway and introduce effector molecules to kill transformed cells could provide an ideal intervention for early-stage cervical cancer or postoperative treatment [29, 30].

Our research team has established the feasibility of affinity selection and identification of affibody using a phage-displayed technology with tumor-associated pathogen-specific target molecules. We have successfully selected affibody molecules targeting HPV16 type E6 and E7 ($Z_{HPV16E6}$ and $Z_{HPV16E7}$) [31, 32], and have confirmed the in vivo and in vitro targeted binding properties of $Z_{HPV16E7}$ alone, or $Z_{HPV16E7}$ conjugated with toxins [33,

34], indicating its potential for further development as an ADC for CC treatment. Considering that HPV16 and 18 types are the two main high-risk types most associated with CC, this study aims to construct a bispecific ADC simultaneously targeting both HPV16 and HPV18 E7 proteins, conjugated with GrB (i.e., bispecific affitoxin), to analyze its inhibitory effects on CC cell growth and evaluate its potential as an ADC for targeted therapy in CC.

Materials and methods

Plasmids, cell lines and animals

Plasmids containing coding sequences, namely, pET21a(+)/$Z_{HPV16\text{-}18E7}$ (bispecific affibody), pET21a(+)/GrB, and pET21a(+)/Zwt (the wild-type affibody without affinity screening) were constructed and maintained in our laboratory.

Human cervical cancer cell lines of SiHa (ATCC (HTB-35), HPV16 type), HeLa (ATCC (CCL-2.1), HPV18 type), and C33A (ATCC (HTB-31), without HPV infection) were purchased from the Cell Bank of the Shanghai Biology Institute, Chinese Academy of Sciences (Shanghai, China), and cultured in RPMI-1640 containing 100 mg/L penicillin and streptomycin (Gibco, USA) and 10% fetal bovine serum (FBS). All cells were maintained at 37 °C in a humidified atmosphere containing 5% CO_2. E. coli BL21 (DE3) super competent cells were prepared in our laboratory.

Four- to six-week-old female nude mice (BALB/c-nu, Certificate No. SYXK- (Zhejiang, China) 2019–0001) for the in vivo anti-tumor assays, six- to eight -week-old nonpregnant female mice (C57BL/6 J, Certificate No. SYXK- (Zhejiang, China) 2020–0014) for the in vivo toxicity tests, and sexually mature New Zealand male rabbits weighing 2.3–2.4 kg (Certificate No. SYXK- (Zhejiang, China) 2019–0009) for the in vivo pharmacokinetics and in vitro stability experiments, were purchased from the Beijing Vital River Laboratory Animal Technology Co. Ltd. All animals were handled according to the Guidelines for the Care and Use of Laboratory Animals and all experimental procedures were approved by the Medical Ethics Committee of Wenzhou Medical University (WYDW 2023–0057).

Reagents and antibody

The following reagents were used: restriction enzymes (*Ned* I and *Xho* I), DNA and protein markers, and 2 × PCR Master Mix (MBI Ferments, Burlington, Ontario, CA); Isopropyl β-D-1-thiogalactopyranoside (IPTG), and Ni–NTA agarose (QIAGEN, Hilden, Germany); RPMI-1640 medium, fetal bovine serum (FBS), penicillin, and streptomycin (Gibco, USA); DeadEnd™ Fluorometric TUNEL System (Promega, USA); CellTiter-Lumi™ Luminescent Cell Viability Assay Kit (Beyotime, China); Fluorescent dye of DyLight-755 (Thermo Fisher Scientific, USA); Prestained protein marker (MBI Ferments, Burlington, Ontario, CA); Hematoxylin–Eosin (HE) Stain Kit (Solarbio, China); Other reagents were analytical reagents (ARs). The following primary antibodies were used: anti-His tag (66,005-1-Ig, Proteintech); anti-GrB and anti-Caspase-3 (ab208586and ab32351, Abcam); anti-Caspase-8 (#4790, Cell Signaling Technology); anti-GAPDH (AB-P-R 001, Good Here); anti-HPV16E7 and anti-HPV18E7 (bs-10446R and bs-10204R, Bioss); anti-E-Cadherin, anti-Vimentin and anti-Snail (#3195 T, #5741 T, #3879 T, Cell Signaling Technology). The following secondary antibodies were used: HRP-labelled goat anti-rabbit IgG, HRP-labelled goat anti-mouse IgG, Cy3-labelled goat anti-mouse IgG, and FITC-labelled goat anti-rabbit IgG (A0208, A0216, A0521, and A0562, Beyotime). The above reagents were purchased from commercial sources.

Plasmid construction

The optimized GrB gene sequence was amplified from plasmid pET21a(+)/GrB, and inserted into N-terminal, middle, or C-terminal of $Z_{HPV16\text{-}18E7}$ (HPV16/18E7 bispecific affibody), respectively, by *Nde* I/*Xho* I digestion from pET21a(+)/$Z_{HPV16\text{-}18E7}$, with a $(Gly_4Ser)_3$ flexible linker to construct three plasmids of affitoxin conjugates, i.e., pET21a(+)/GrB-$Z_{HPV16E7\text{-}HPV18E7}$ (pET21a(+)/GrB-$Z_{16\text{-}18}$ for short), pET21a(+)/$Z_{HPV16E7}$-GrB-$Z_{HPV18E7}$ (pET21a(+)/Z_{16}-GrB-Z_{18} for short), pET21a(+)/$Z_{HPV16E7\text{-}HPV18E7}$-GrB(pET21a(+)/$Z_{16\text{-}18}$-GrB for short), and plasmid pET21a(+)/Zwt-GrB (as off-target control).

Protein preparation

Cells of the E. coli BL21 (DE3) super competent cells were transformed with above plasmids under the induction of 1 mM IPTG (Sigma, USA) for the expression of the bispecific affitoxins. The expressed products were purified by a Ni^{2+}-chelated affinity column (Qiagen, Hilden, Germany) and verified by sodium dodecyl sulfate–polyacrylamide gel electrophoresis (SDS-PAGE) and western blot. Websites of https://webexpasy.org/ and http://galaxy.seoklab.org were employed respectively for analyzing physicochemical properties and spatial structures of three conjugates.

SPR assay

A Biacore T200 instrument (Cytiva, USA) was used to detect the binding interaction between the bispecific affitoxins and the two targets of HPV16E7 and HPV18E7. Previously prepared and purified HPV16E7 or HPV18E7 (10 μg/ml) in our laboratory was immobilized respectively on the flow-cell surfaces of sensor chip (CM5) according to the manufacturer's instructions. The expressed two bispecific affitoxins with 1: 2 serial dilution

(300 μg/ml, 150 μg/ml, 75 μg/ml, 37.5 μg/ml, 18.75 μg/ml, respectively) were injected over all surfaces at a flow rate of 30 μl/min for 2 min, followed by dissociation for 10 min. The concentration with the valid Resonance Unit was determined for further analysis of the binding to the target protein E7 in each group. Data evaluation and estimation of the kinetic parameters k_a, k_d, K_D were performed using the software *TraceDrawer*1.1 (Biacore T200 evaluation software).

Indirect immunofluorescence assay

CC cell line of SiHa (HPV16 +), or HeLa (HPV18 +), or C33A (HPV-, as control) co-cultured respectively with bispecific affitoxins (150 μmol/ml) for 6 h on slides was fixed with 4% paraformaldehyde for 20 min at 37 °C and blocked in buffer (PBS containing 5% FBS) at 4 °C overnight. The slides were incubated with primary antibodies of anti-His tag (1: 500), anti-HPV16E7 (1: 250), or anti-HPV18E7 (1: 250), respectively, at 4 °C overnight, and then incubated with the corresponding FITC-conjugated goat anti-mouse IgG (H + L) or Cy3-conjugated goat anti-rabbit IgG (H + L) (diluted 1: 1000) at 37 °C for 1 h. The cell nuclei were stained with DAPI at 37 °C for 5 min. The cells were analysed by a confocal fluorescence microscope (STELLARIS 5, Leica, Germany).

Cell viability assay

Cell Counting Kit-8 (CCK-8) assay was applied for determining the IC_{50} of bispecific affitoxins on SiHa and HeLa cell. Briefly, 8×10^3 cells /well were seeded into 96-well plate. After co-cultured for 72 h with the gradient dilutions of affitoxins in 200 μg/mL, 100 μg/mL, 50 μg/mL, 25 μg/mL, 12.5 μg/mL, or 6.25 μg/mL, respectively, the plate was added with 10 μl CCK-8 solution into each well, and then cultured for 2 h at cell culturing condition followed by measurement of OD value at 450 nm wavelength. Additionally, CellTiter-Lumi™ Luminescent Cell Viability Assay Kit was applied for determining the cell viability. Briefly, 8×10^3 cells of SiHa, HeLa, or C33A/well with 100 μg/mL affitoxins, or with 5 μg/mL cisplatin (as a positive drug control) were seeded into 96-well plate, and co-cultured for 72 h. The subsequent actions were performed according to the manufacturer's instructions.

Cell apoptosis assay

A DeadEnd™ Fluorometric TUNEL System (Promega, USA) was applied for evaluating cell apoptosis. Briefly, 8×10^3 cells of SiHa, HeLa, or C33A/well co-cultured with 100 μg/mL bispecific affitoxins for 18 h were collected and re-suspended at 3×10^6 cells/mL. The subsequent actions were performed according to the manufacturer's instructions. TUNEL-positive cells were counted under a fluorescence microscope. Apoptosis-related molecules of cleaved caspase-8, and cleaved caspase-3 were evaluated by western blot.

Cell migration assay

Wound healing assay and transwell assay were used for detecting cell migration. Briefly, (ⅰ) Cell lines of SiHa, HeLa, or C33A were plated in 12-well culture plates to achieve 90% confluence, and then a vertical wound was performed using a 0.1 μl pipette tip. The cells were co-cultured with bispecific affitoxins (1.0 μM) with FBS-free medium for 12, or 24 h, respectively. Images were captured at indicated time to assess wound closure rate. (ⅱ) 1×10^5 cells /well co-cultured with affitoxins (1.0 μM) were seeded in the chamber with FBS-free medium for incubation at 37 °C in a 5% CO_2 atmosphere for 24 h. Cells adhered to the upper surface of the chamber membrane were removed and invaded cells were stained with 0.4% crystal violet acetate overnight. The stained cells were photographed for quantitative analysis. EMT-related molecules of E-cadherin, Vimentin, and Snail were detected by western blot.

Western blot assay

Cell lysates were separated by 10% sodium dodecyl sulfate–polyacrylamide gel electrophoresis (SDS-PAGE) and then transferred to polyvinylidene fluoride (PVDF) membrane. After being blocked in 5% milk (w/v) at room temperature for 1 h, the primary antibodies (1: 1000) against the indicated antigens in cells were added for incubation at 37 °C for 2 h, and the corresponding HRP-labelled anti-mouse IgG or HRP-labelled anti-rabbit IgG was used as the secondary antibody (1: 5000) for incubation at 37 °C for 1 h. Protein bands were visualized using a Chemiluminescence Detection Kit (Pierce, Rockford, IL) according to the manufacturer's instructions.

NIR optical imaging

1×10^7 SiHa or HeLa cells mixed with Matrigel were injected subcutaneously into the right armpit of the back of BALB/c nude mice (n = 5 per group). On day 13, tumors with 100 mm^3 were formed and RT-PCR was used to identify oncogene E7 in the isolated tumor tissues. Near-infrared (NIR) optical imaging was applied to investigate the in vivo tumour-targeting ability of the bispecific affitoxin. Briefly, affitoxin was labeled with amaleimide derivative of DyLight-755 (62,278, Thermo Fisher Scientific, USA) and the imaging system of Perkinelmer IVIS LuminaX5 was used to check the affitoxin-DyLight-755 on SDS-PAGE under darker conditions. When tumour size reached 400 mm^3, 100 μL of affitoxin-DyLight-755 (50 μM) was injected into the mice via the tail vein, and fluorescence imaging was performed using an NIR imaging system (CRi Maestro 2.10, USA).

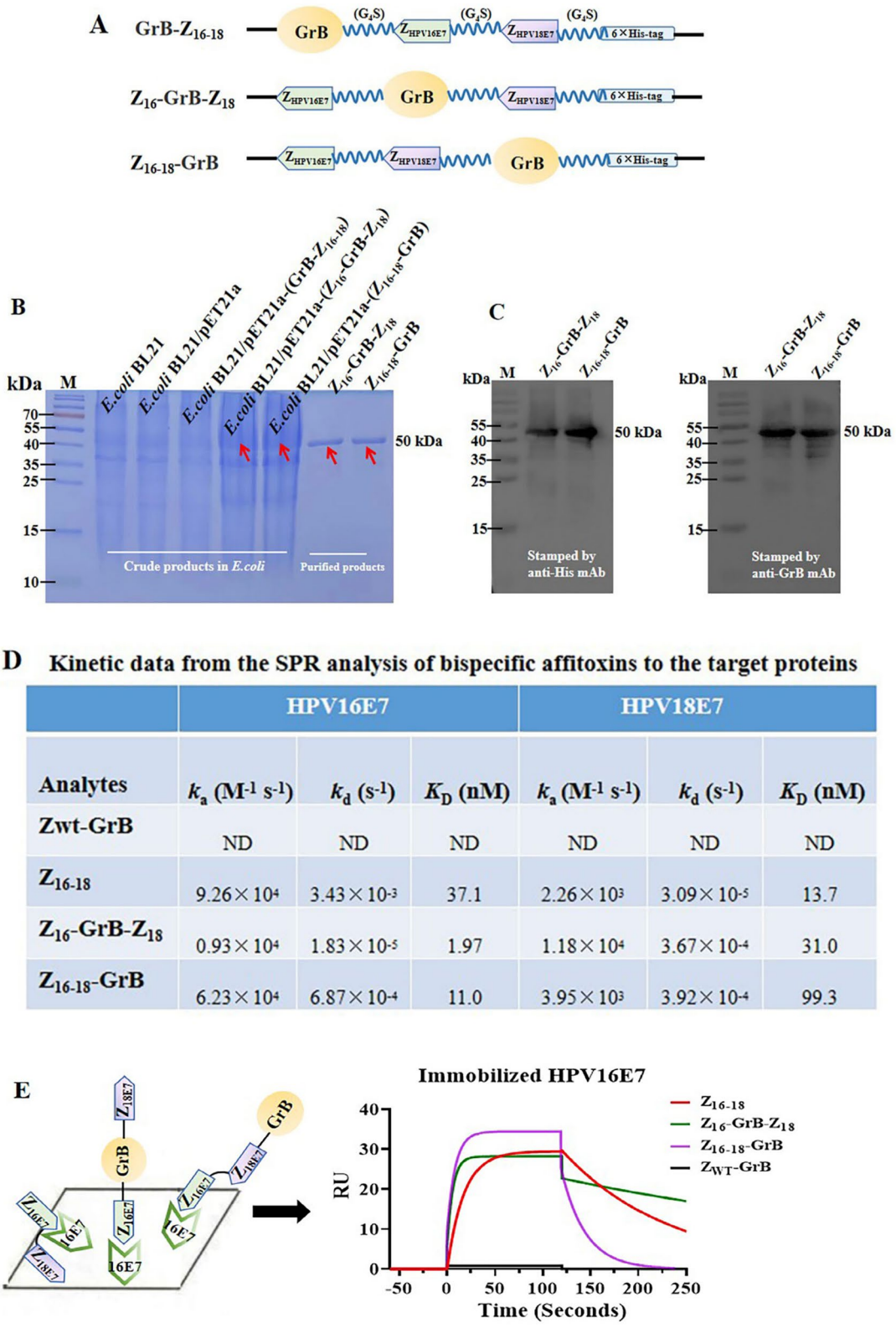

	HPV16E7			HPV18E7		
Analytes	k_a (M^{-1} s^{-1})	k_d (s^{-1})	K_D (nM)	k_a (M^{-1} s^{-1})	k_d (s^{-1})	K_D (nM)
Zwt-GrB	ND	ND	ND	ND	ND	ND
Z_{16-18}	9.26×10^{4}	3.43×10^{-3}	37.1	2.26×10^{3}	3.09×10^{-5}	13.7
Z_{16}-GrB-Z_{18}	0.93×10^{4}	1.83×10^{-5}	1.97	1.18×10^{4}	3.67×10^{-4}	31.0
Z_{16-18}-GrB	6.23×10^{4}	6.87×10^{-4}	11.0	3.95×10^{3}	3.92×10^{-4}	99.3

Fig. 1 (See legend on next page.)

(See figure on previous page.)

Fig. 1 Prepared bispecific affitoxins with double-targeting affinity. **A** Construction model of three bispecific affitoxins. **B** Production and purification of bispecific affitoxins. Red arrows indicated the expressed and purified products of Z_{16}-GrB-Z_{18} and $Z_{16\text{-}18}$-GrB, while not expression of GrB-$Z_{16\text{-}18}$ in E. coli. **C** Confirmation of immunoreactivity of bispecific affitoxins by western blot. **D** Kinetic parameters of bispecific affitoxins interacting with the targets in SPR assay. ND = not determined; k_a = association rate constant; k_d = dissociation rate constant; K_D = dissociation constant. **E–F** The specific binding of bispecific affitoxins to target E7 by SPR. To the left are schematic representations of affibody Z_{16E7} in each analyte binding to HPV16E7 immobilized on the chip **E**, and of affibody Z_{18E7} in each analyte binding to HPV18E7 immobilized on the chip **F**. To the right are the actual measured response signals. Z_{WT}-GrB served as off-target affitoxin control

Anti-tumor growth in vivo

When the tumour volume reached 50 mm^3, bispecific affitoxin (100 nmol/kg) or cisplatin (13 nmol/kg, as a positive control) were injected into the mice (n = 5) by the tail vein 5 times in total at 6-day intervals. Tumour initiation, progression and mouse weight were recorded every 6 days until day 31, and then the mice were sacrificed to isolate the tumors for comparisons of their weight and size.

Acute toxicity evaluation in vivo

Non-pregnant female C57BL/6 J mice weighting 20–24 g (n = 5 per group) were intravenously injected with bispecific affitoxin (8 μg/g). After 24 h, mice were anesthetized with isoflurane and blood samples were collected at the eye socket. Blood samples in anticoagulant tube (containing EDTA-K2) were subjected to routine blood test by a full-automatic hematology analyzer, and the serum from blood samples were subjected to liver and kidney function tests by a full-automatic biochemical analyzer. Liver and kidney organs were separated from euthanized mice and immersed in 4% paraformaldehyde to prepare tissue sections for HE staining according to the manufacturer's instructions.

Evaluation of pharmacokinetics and stability

Enzyme linked immunosorbent assay (ELISA) was used for the evaluation of the pharmacokinetics in the serum collected at the indicated times of 0 min, 5 min, 15 min, 30 min, 1 h, 2 h, 6 h, 12 h, 24 h, 48 h, and 72 h via ear vein from female healthy NZW rabbits weighting 2.3–2.4 kg (n = 3) administrated with bispecific affitoxin (4 mg/kg) by intravenous injection, and the stability of bispecific affitoxin (125 μg/mL) co-incubated with the plasma from rabbit. Briefly, high-adhesion 96-well flat-bottom microtiter plates (Corning, Lowell, MA) were coated overnight at 4 °C with HPV16E7 or HPV18E7 (prepared and maintained in our laboratory, 0.25 μM/well), respectively. After blocked at 37 °C for 2 h with 5% skim milk in PBST and washed with PBST, the collected serum (1: 100) or plasma-affitoxin (equivolume mixture) was added into plates, respectively, for the incubation at 37 °C for 2 h. After washing, anti-His tag (6 × histidine in affitoxin) mAb (1: 5000) was added for incubation, then followed HRP-conjugated anti-mouse IgG (1: 5000) for incubation, at 37 °C for 2 h, respectively. Colour development of chromogenic substrate TMB (OPD; Sigma) was employed, and the results were recorded at 450 nm using an automated ELISA plate reader (Bio-Tek EL × 800).

Statistical analysis

Data are expressed as the means ± standard deviations (SDs). All comparisons were tested for significance by one-way ANOVA. Differences with $P \le 0.05$ were considered significant. Statistical analysis was performed with GraphPad Prism 5.0 software.

Results

Prepared bispecific affitoxins with double-targeting affinity

In order to simultaneously cover HPV16 and 18 major carcinogenic types, three conjugation patterns of bispecific affitoxins were designed (shown in Fig. 1A), and online prediction showed their consistent spatial structures and physicochemical properties. After transformation to E. coli BL21(DE3) with three plasmids corresponding to three bispecific affitoxins, two bispecific affitoxins with 50 kDa of Z_{16}-GrB-$_{18}$ and $Z_{16\text{-}18}$-GrB were produced with IPTG induction, but not the conjugate of GrB-$Z_{16\text{-}18}$ (i.e., GrB fused into $Z_{16\text{-}18}$ N-terminal), indicating that the fusion location between molecules may cause a codon bias in E. coli leading to non-expression of expected protein (Fig. 1B). The expressed Z_{16}-GrB-$_{18}$ and $Z_{16\text{-}18}$-GrB could be purified by Ni^{2+} affinity chromatography, and recognized by a anti-His-tag mAb, or by anti-GrB mAb, respectively (Fig. 1B–C), which confirmed their immunobinding property. SPR analysis was used to verify the kinetic binding of Z_{16}-GrB-$_{18}$ and $Z_{16\text{-}18}$-GrB to the targets of HPV16E7 and HPV18E7. The binding of each analyte with serial dilution to E7 and control parameters were shown in SFig. 1A–B. Under the condition of each analyte with the determined concentration of 300 μg/ml, the kinetic parameters, k_a and k_d as well as the dissociation equilibrium constant (K_D), were measured using the binding-curve evaluation software *TraceDrawer* (Fig. 1D), showing that the bispecific affibody of $Z_{16\text{-}18}$ has faster binding and dissociation rates with the targets compared with the bispecific affitoxins of Z_{16}-GrB-$_{18}$ and $Z_{16\text{-}18}$-GrB, especially for Z_{16}-GrB-$_{18}$ with the strongest binding. The obtained sensorgrams from the biosensor analysis showed that both Z_{16}-GrB-$_{18}$ and $Z_{16\text{-}18}$-GrB had preserved functionality of bispecific binding to HPV16E7 and HPV18E7 like the bispecific affibody of $Z_{16\text{-}18}$ (Fig. 1E–F).

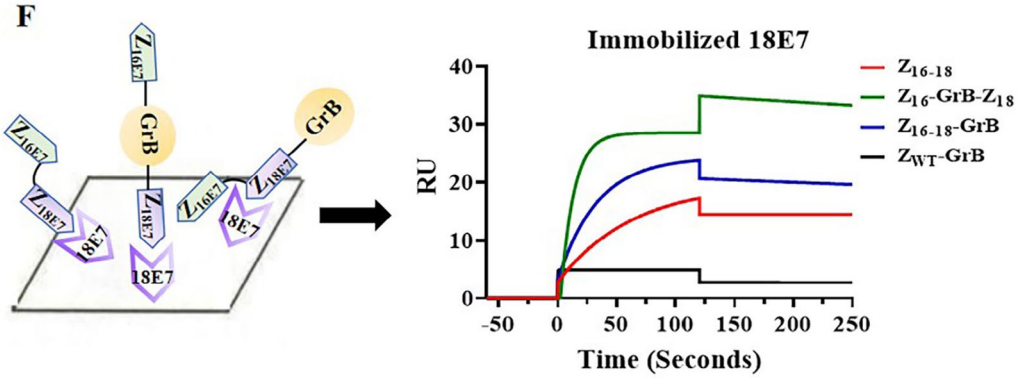

Fig. 1 (continued)

Binding of bispecific affitoxins to HPV16 and 18 positive CC cells

A confocal immunofluorescence assay was applied to evaluate the simultaneous binding of bispecific affitoxins to CC cell lines of HPV16 and 18 types. The results showed that significant red fluorescence signals could be observed in SiHa (HPV16 +) (Fig. 2A) and HeLa (HPV18 +) cells (Fig. 2B) incubated with Z_{16}-GrB-$_{18}$, or Z_{16-18}-GrB, or Z_{16-18}, respectively, but not in C33A (HPV-) cells (SFig. 2) indicating the entry of both bispecific affitoxins and bispecific affibody into the target cells. Additionally, there were the co-localization between red fluorescence (affitoxins or affibody) and green fluorescence (E7), but not in Zwt-GrB group, further indicating the specificity of affitoxins or affibody to the target molecule in cells.

Inhibition of bispecific affitoxins in HPV16 and 18 positive CC cells

The growth inhibition of bispecific affitoxins in both SiHa and HeLa CC cells was evaluated by CCK-8 for their anticancer activity. Both Z_{16}-GrB-$_{18}$ and Z_{16-18}-GrB exhibited a nearly identical growth inhibition, with IC_{50} (half-maximal inhibitory concentration) values of 1.978 and 1.937 μM in SiHa cells, while 2.191 and 2.148 μM in HeLa cells, indicating a more desirable inhibitory effect than bispecific affibody Z_{16-18} with IC_{50} of 4.845 μM in SiHa and 3.9 μM in HeLa cells (Fig. 3A). Similarly, bispecific affitoxins of Z_{16}-GrB-$_{18}$ and Z_{16-18}-GrB significantly decreased cell viability compared with bispecific affibody Z_{16-18} in both SiHa and HeLa cells (Fig. 3B), which exhibited an advantage of affibody fusion with GrB. Cisplatin, as a clinical medication for advanced CC to be used as a positive control, showed almost 100% of inhibition, indicating the need for further optimization of affitoxin, or affibody for their application.

Apoptosis induced by bispecific affitoxins on HPV16 and 18 positive CC cells

Because of GrB as an apoptosis induction effector, apoptosis induced by bispecific affitoxins in both SiHa and HeLa CC cells was evaluated by a TUNEL assay. The results showed that the rate of apoptosis cells in bispecific affitoxins of Z_{16}-GrB-$_{18}$ and Z_{16-18}-GrB groups in SiHa (Fig. 4A) and HeLa (Fig. 4B) cells was significantly higher than that in Z_{16-18} or Z_{WT}-GrB group, respectively ($P<0.05$), whereas no obvious apoptosis was observed in control C33A (Fig. 4C) cells. Western blot analysis showed significant increases in the protein levels of the pro-apoptotic factor cleaved caspase-8 and cleaved caspase-3 (Fig. 4D) in Z_{16}-GrB-$_{18}$-, Z_{16-18}-GrB-, and Z_{16-18}-treated SiHa and HeLa cells, whereas less evident increases in Z_{WT}-GrB- and mock- treated cells, indicating that the apoptosis inducing by bispecific affitoxins and bispecific affibody was achieved by caspase-8/3 activation pathway. Notably, bispecific affibody Z_{16-18} (without conjugation with GrB) also induced apoptosis, but the apoptosis degree was lesser than bispecific affitoxin groups ($P<0.05$), indicating the superiority of specific targeting cytotoxicity by affibody cooperated with GrB.

Suppression of migration by bispecific affitoxins in HPV16 and 18 positive CC cells

Cancer metastasis and recurrence are the difficulties for CC treatment. Here, the suppressing migration of bispecific affitoxins and affibody was investigated. Both of wound healing and transwell assays demonstrated the same decreased cell migration by bispecific affitoxins (Z_{16}-GrB-$_{18}$ and Z_{16-18}-GrB) and bispecific affibody (Z_{16-18}) in both SiHa and HeLa cells (Fig. 5A–D), indicating the same ability of affitoxin and affibody in suppressing cell migration which proved the specific blockage function of affibody. Given the strong link between tumor cell migration and epithelial-mesenchymal transitions (EMT), the related factors with EMT were assayed using western blot, and the results showed that expressed level

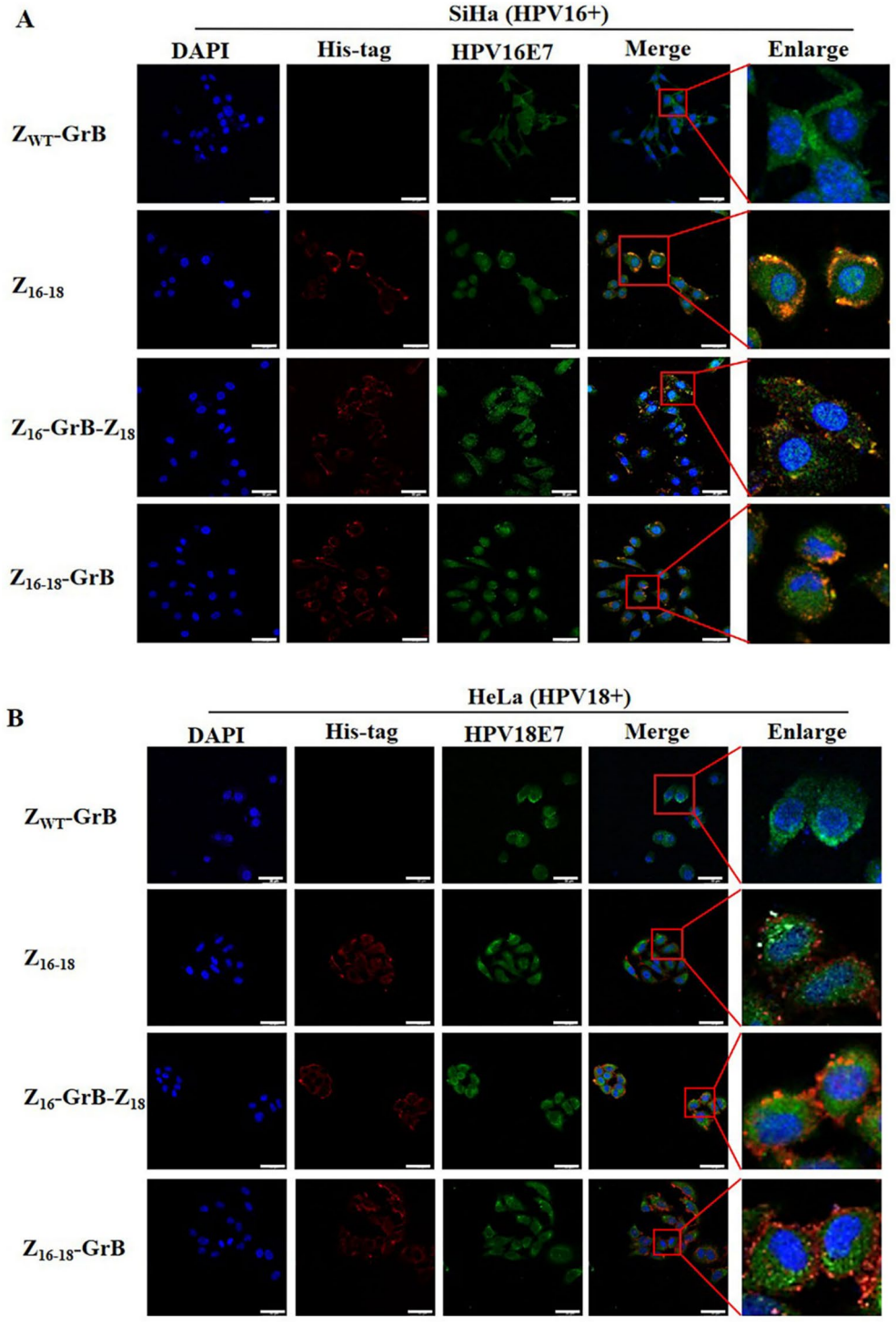

Fig. 2 Binding of bispecific affitoxins to HPV16 and 18 positive CC cells. **A–B** The subcellular co-localization of Z_{16}-GrB-Z_{18}, or Z_{16-18}-GrB, or Z_{16-18} with E7 in SiHa cells **A** and in HeLa cells **B**. Blue signals: cell nucleus stained by DAPI; Red signals: affitoxins or affibody stained by anti-His-tag resulting from the bispecific affitoxins (Z_{16}-GrB-Z_{18} and Z_{16-18}-GrB) and bispecific affibody (Z_{16-18}) fused with 6 × histidines tag; Green signals: HPV16- or HPV18-E7 stained by anti-E7 monoclonal antibody. Fluorescence signals were observed under a confocal fluorescence microscope. Bar = 50 μm

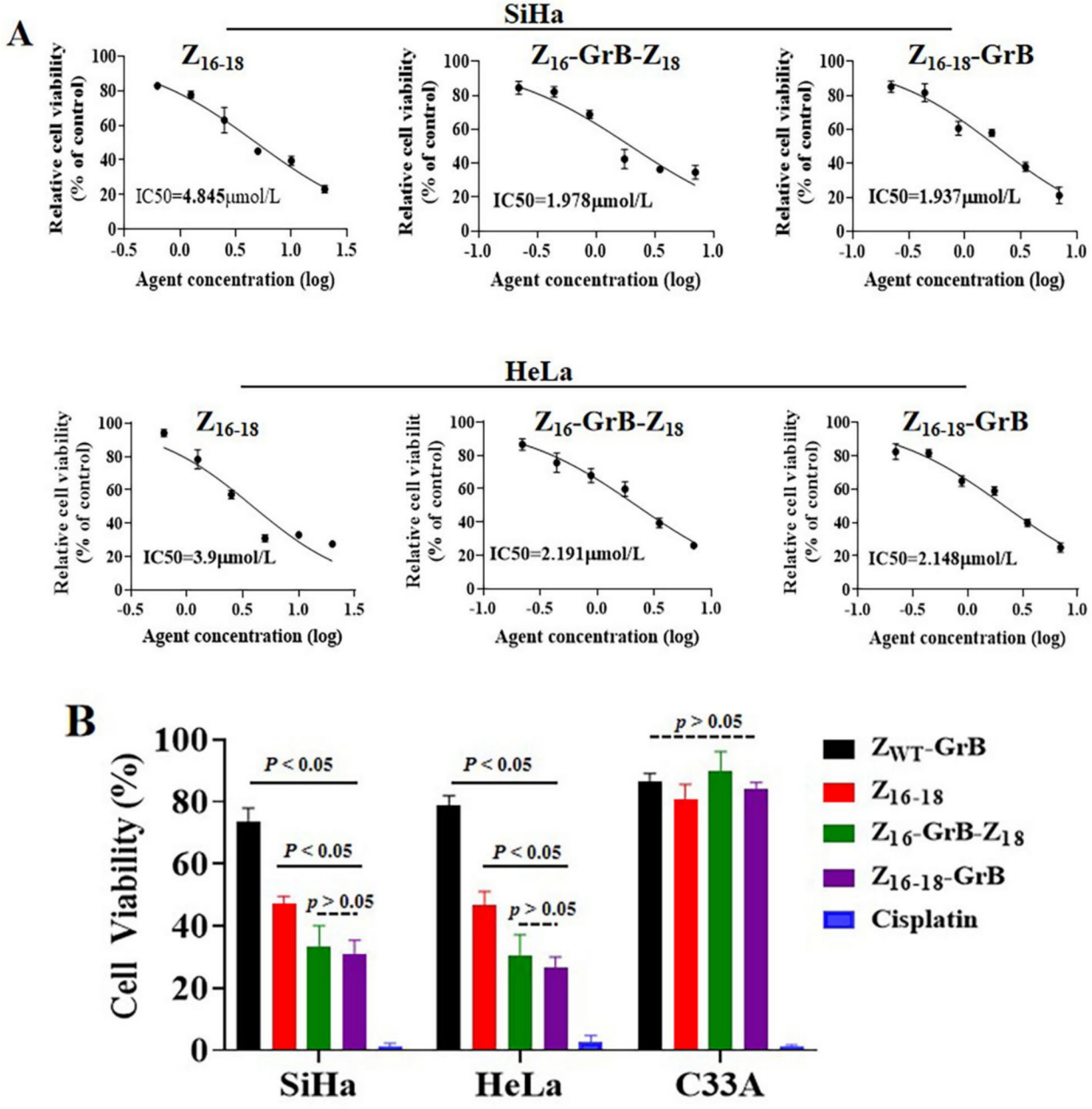

Fig. 3 Bispecific affitoxins inhibited cell viability in SiHa and HeLa cells. **A** Determination of IC_{50} of Z_{16}-GrB-$_{18}$, Z_{16-18}-GrB, and Z_{16-18} at 72 h by CCK-8. **B** Significantly reduced cell viability by bispecific affitoxins of Z_{16}-GrB-$_{18}$ and Z_{16-18}-GrB at 72 h using CellTiter-Lumi™ luminescence assay. Cisplatin served as the positive agent control. C33A served as off-target cell control without HPV. Data are presented as the mean ± SEM (n = 3)

of E-cadherin, the marker of epithelial cell, was increased obviously, while Vimentin and Snail, the markers of mesenchymal cell, were decreased significantly (Fig. 5E), indicating the possible regulation of EMT process mediated by bispecific affitoxins and affibody.

Accumulation of bispecific affitoxin to tumor tissues in vivo

The oncogenic protein HPV E7 subjected to mRNA (315 bp for HPV16E7, 269 bp for HPV18E7) could be detected using RT-PCR from the tumour tissues in SiHa- or HeLa-bearing nude mice (Fig. 6A). All agents used for near-infrared fluorescence imaging in vivo including bispecific affitoxin (Z_{16-18}-GrB), bispecific affibody (Z_{16-18}), and affitoxin control (Z_{WT}-GrB) could be labeled with DyLight-755 (Fig. 6B). After injection of agents-DyLight-755 for 4 h, obvious red fluorescent signals were presented at the tumor site in groups of Z_{16-18}-GrB-DyLight-755 and Z_{16-18}-DyLight-755 (Fig. 6C), but not in Z_{WT}-GrB-DyLight-755 group, demonstrating the same targeted enrichment of affitoxin and affibody.

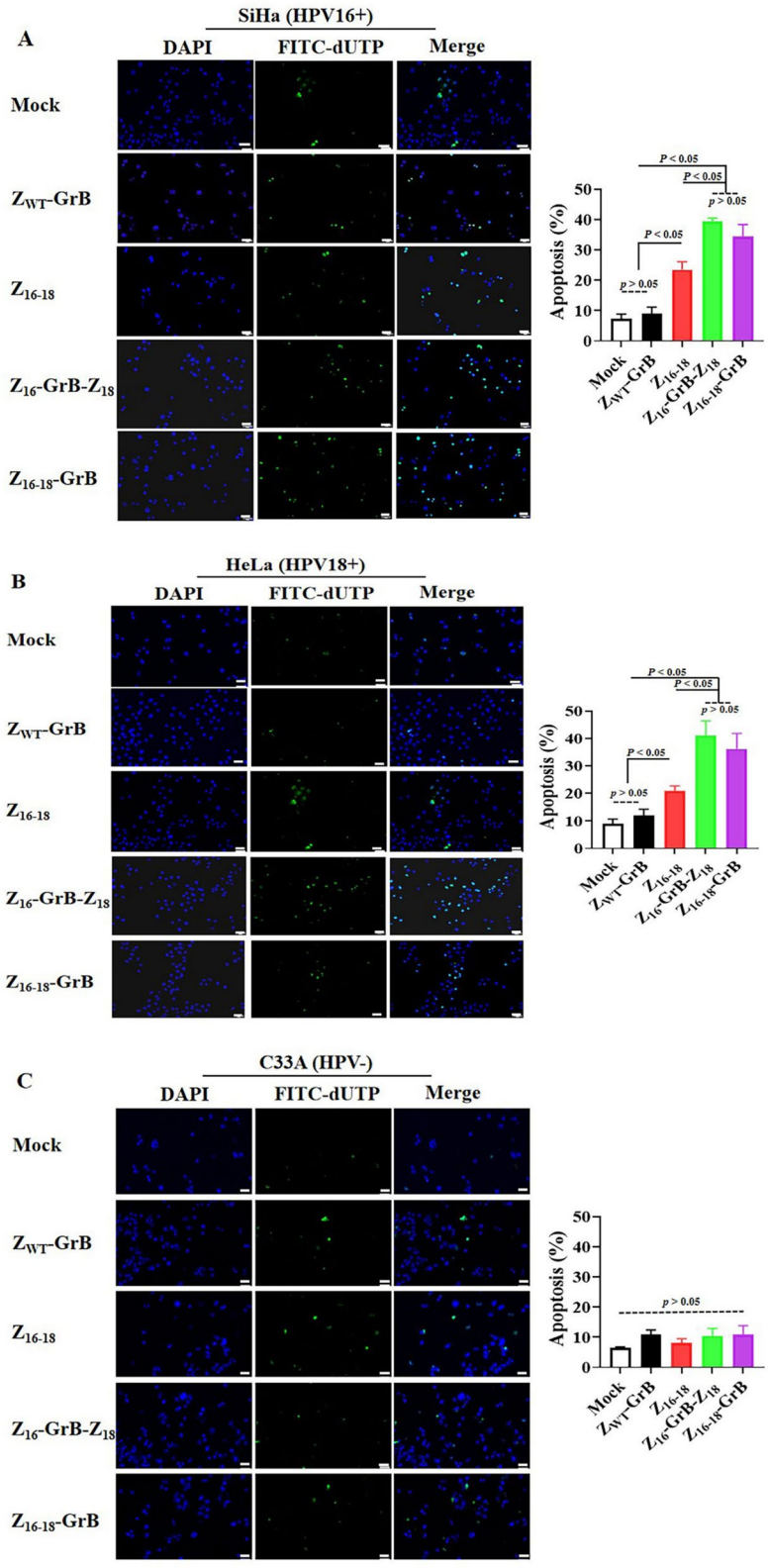

Fig. 4 Induced cell apoptosis by bispecific affitoxins in SiHa and HeLa cells. **A–C** Apoptosis detection and quantitative analysis by Fluorometric TUNEL method in SiHa cells **A**, HeLa cells **B**, and C33A cells **C**. Bar = 50 μm. **D** Analysis of apoptosis-related factors by western blot in SiHa and HeLa cells

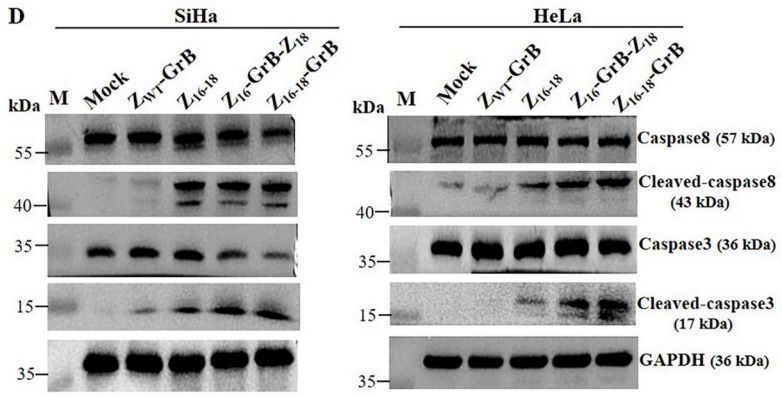

Fig. 4 (continued)

Inhibition of tumor progression by bispecific affitoxin in vivo

The BALB/c-un mice were used for the subcutaneous transplant tumors-modeling to evaluate the anti-tumor activity of bispecific affitoxin in vivo. The experiment workflow was showed in Fig. 7A. The process of tumor development in mice was recorded at 7 day intervals, showing a significant time-dependent tumor growth, and a progressive rapid growth after 13 days in negative control groups (mock and Z_{WT}-GrB), whereas a significant inhibition of tumor growth in groups of Z_{16-18} and Z_{16-18}-GrB was observed, especially a more obvious anti-tumor effect in Z_{16-18}-GrB group compared with Z_{16-18} group. Cisplatin group (as positive control) completely suppressed tumor growth (Fig. 7B for SiHa cells, Fig. 7G for HeLa cells). The mouse weight was weighed at 6-day intervals and the results showed that all mice after administration with agents had kept broadly the same in body weight but except cisplatin group, indicating the side effect of cisplatin whereas the relative safety of the agents (Fig. 7C for SiHa cells, Fig. 7H for HeLa cells). By comparing the isolated tumor size (Fig. 7D for SiHa cells, Fig. 7I for HeLa cells), volume (Fig. 7E for SiHa cells, Fig. 7J for HeLa cells), and weight (Fig. 7F for SiHa cells, Fig. 7K for HeLa cells) on day 31, a smaller size and lighter weight of tumour tissues could be observed in mice of Z_{16-18}-GrB group than Z_{16-18} group, indicating an advantage of co-suppressing tumor growth of affibody conjugation with GrB. As expected, cisplatin exhibited the most potent inhibition function.

No production of acute toxicity by bispecific affitoxin in vivo

Healthy C57BL/6 J mice were administrated with Z_{16-18}-GrB or Z_{16-18} by intravenous injection for evaluating the potential acute toxicity in vivo. The experiment workflow was showed in Fig. 8A. After 24 h, routine blood test, liver/kidney function analysis, and H&E staining were used for the evaluation of body condition. The results showed that there were no significant changes in blood cells (RBC, WBC, PLT), HGB, five WBC classification (NEUT, EO, BASO, LYMPH, MONO) in Z_{16-18}-GrB- or Z_{16-18}-treated mice (Fig. 8B). Meanwhile, no damages were produced in Z_{16-18}-GrB- or Z_{16-18}-treated mice as indicated by liver and kidney function indexes (Fig. 8C), and by H&E staining (Fig. 8D). Therefore, the administration with Z_{16-18}-GrB or Z_{16-18} would not introduce any significant toxicity to the mice.

Investigation of pharmacokinetics and stability of bispecific affitoxin

Healthy New Zealand rabbits were used for evaluating bispecific affitoxin pharmacokinetics and stability by ELISA. The experiment workflow was showed in Fig. 9A. The results showed that the distribution of bispecific affitoxin in the blood was gradually decreased over time after intravenous administration (Fig. 9B), and the content had significantly decreased at 4 h in blood, speculating that the bispecific affitoxin may have accumulated towards the tumor site or metabolized by kidney, which was in accord with the imaging results of Fig. 6C mentioned before. After 24 h, only trace bispecific affitoxin in blood can be detected. While, the co-incubated bispecific affitoxin with rabbit blood in vitro still remained relatively stable with time (Fig. 9C), and after co-incubation for 6 h, bispecific affitoxin began a slow-decrease but still remained at a high level to 72 h, indicating almost no protease disruption from the blood on bispecific affitoxin with a relative stability.

Discussion

Immunotoxin, often referred to as "biological missile", is conjugate formed by linking highly specific monoclonal antibody (mAb) with potent toxic molecule, which deliver the toxin directly to tumor cells for killing, resulting in the purpose of targeted tumor therapy[35]. Currently, several immunotoxins targeting specific cancer biomarkers are under FDA review, with some already in

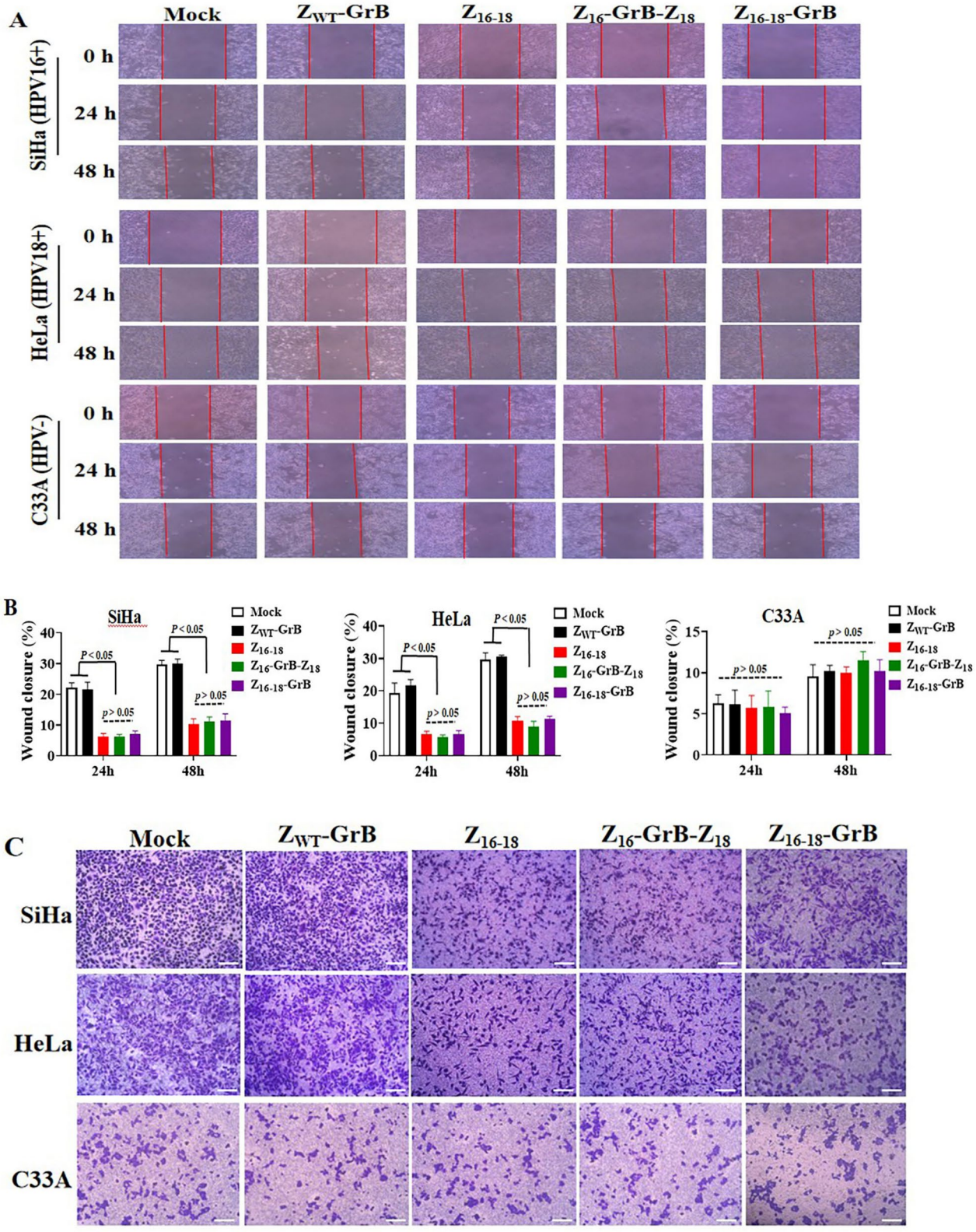

Fig. 5 Suppressed cell migration by bispecific affitoxins and affibody in SiHa and HeLa cells. **A** The detection of cell migration by wound healing assay (magnifying × 10). **B** Quantitative analysis of **A** by Image J. **C** The detection of cell migration by transwell assay (Bar = 200 μm). **D** Quantitative analysis of **C** by counting the non-migrated cells. Data are presented as the mean ± SEM (n = 3). **E** The detection of EMT-related factors by western blot. GAPDH served as loading control of protein

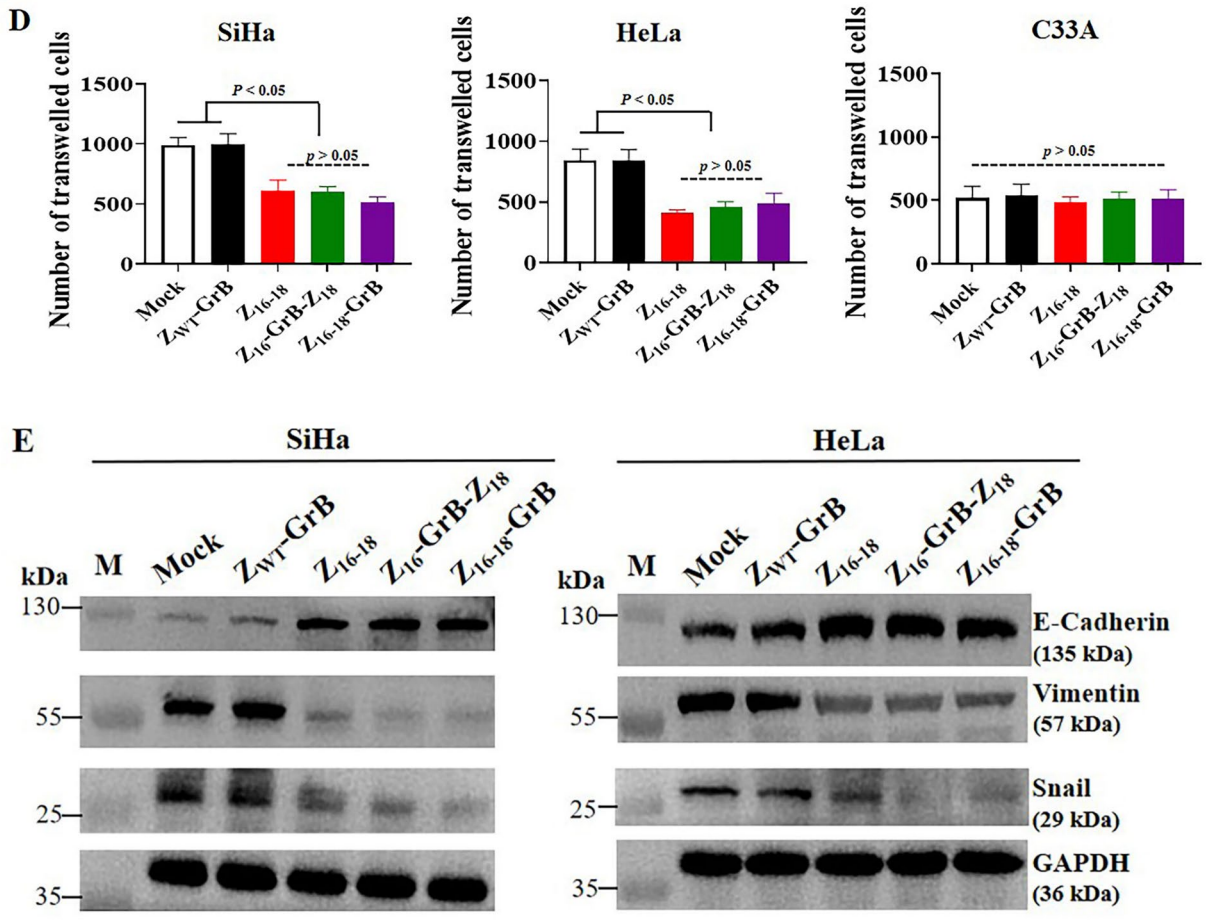

Fig. 5 (continued)

clinical trials. For instance, MT-5111, is an immunotoxin that targets HER2 for the treatment of HER2-positive tumors and currently undergoing Phase I clinical trials [36]; Lumoxiti, an immunotoxin against CD22, is indicated for the treatment of relapsed or refractory hairy cell leukemia (HCL) and has received approval in both the European Union and the United States [37]. Notably, the FDA approved Tivdak (Tisotumab vedotin) in 2021, marking a significant advancement in targeted therapy for recurrent or metastatic cervical cancer (CC) patients during or after chemotherapy [38]. This ADC targets tissue factor (TF) and delivers the cytotoxic agent MMAE (Monomethyl auristatin E) directly into cancer cells to play its lethal effect, demonstrating promising prospects for CC targeted therapy [39]. The persistent infection of HR-HPV is closely associated with the development of CC. However, there are currently no targeted therapeutic agents specifically addressing HPV in CC. Therefore, the present study aims to design an ADC that targets both HPV16 and HPV18, the two most prevalent high-risk types, addressing a significant clinical need and therapeutic opportunity.

ADCs represent a novel therapeutic modality with immense potential of paradigm shift in tumor chemotherapy. Traditional immunotoxins based on mAb are characterized by large molecular sizes, strong immunogenicity, poor tissue penetration, and hard to reach the focus. In contrast, small molecular affibody overcome these limitations to enter cells by dynamin- and caveolin-1-dependent endocytosis pathway[12], thereby addressing the bottleneck of cellular uptake that mAb face, and more to the point, the affibody-based ADC still retains targeted binding characteristics and significant inhibition of tumor growth [33, 34]. Unlike the complexity associated with mAb production, affibody can be produced on a large scale in prokaryotic expression systems. Based on the achieved HPV16E7 and HPV18E7 specific affibodies by affinity screening in our previous work, the present study has constructed three ADC combinations by the linker of flexible peptides. Predictions from the online tool (http://galaxy.seoklab.org) indicate that each molecular among the three ADC combinations do not overlap, with three α-helical regions of affibody while predominantly β-folding of GrB, which consistent with

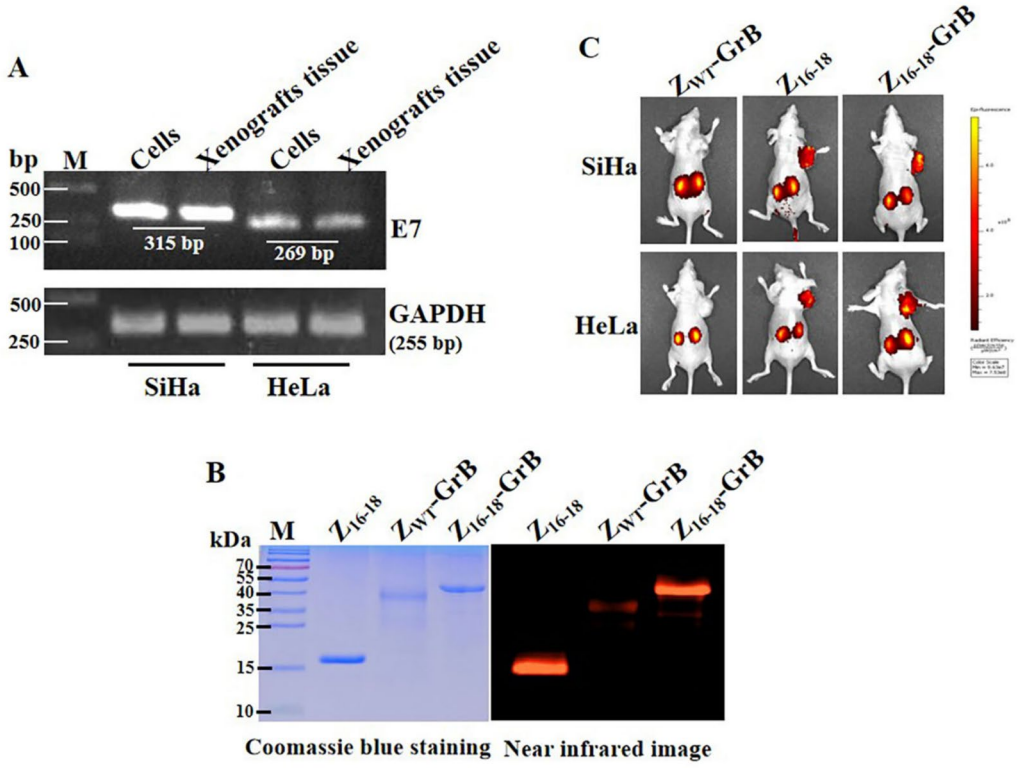

Fig. 6 The accumulation of bispecific affitoxin and affibody to tumor tissues in vivo. **A** The detection of oncoprotein E7 gene in tumor tissues from SiHa- or HeLa-bearing mice by RT-PCR. GAPDH served as reference gene. **B** The confirmation of DyLight-755 labeled bispecific affitoxin and affibody under NIR optical imaging. **C** The enrichment of bispecific affitoxin- and affibody-DyLight-755 at tumor tissues under NIR optical imaging in SiHa- and HeLa-bearing mice (n = 3)

theoretical expectations. Antibody-based drugs typically require a positive charge for effective liquid-phase endocytosis or pinocytosis, thus the environmental pH must be below the isoelectric point (pI) of the drug. Analysis of a prediction on website (https://web.expasy.org/protparam/) indicates that the physicochemical properties of the three ADC agents are similar, with pI values exceeding 7.75 (above the physiological pH range), which suggests that, theoretically, these agents would demonstrate favorable absorption properties in vivo. However, it is intriguing that the conjugates of $Z_{16\text{-}18}$-GrB (GrB fused to the "C"-end of affibody) and Z_{16}-GrB-$_{18}$ (GrB fused to the middle of affibody) were effectively expressed in the prokaryotic expression system and exhibited corresponding immunological binding characteristics, but the conjugate of GrB-$Z_{16\text{-}18}$ (GrB fused to the "N"-end of affibody) failed to yield the expected product. This raises questions regarding whether the conjugation of GrB to the "N"-end of affibody interferes with the signal peptide or whether it induces codon bias. These issues warrant further investigation in subsequent researches.

One of the hallmark features of HPV-induced carcinogenesis is the persistent expression of the E7 oncogenic protein, which is maintained throughout the tumorigenesis process and sustains the cancer phenotype. Our findings demonstrate that both E7-specific affibody and E7-affibody-based affitoxins can target E7 in CC cells, inhibiting cell viability. In tumor-bearing mice treated with these agents, the agents accumulated in the tumor sites, while the E7 oncogene was not detected in major organs outside the tumor, indicating that the agents probably suppressed tumor cell metastasis. HPV infects basal layer cells where virus proliferates and these basal cells exhibit stem cell-like properties with lifelong capacity for division which contribute to the high recurrence rates of CC. Post-surgical recurrence and metastasis of CC result in a mortality rate of 29–38%, highlighting the necessity of eliminating HPV infection or blocking HPV malignant transformation as a primary goal in CC treatment. Tumor cell metastasis is linked to the epithelial-mesenchymal transition (EMT) process. Our findings demonstrate that CC cells treated with affibody or affitoxins exhibited an increase in the epithelial marker E-Cadherin, while a decrease in the mesenchymal marker Vimentin and the transcription factor Snail, indicating an inhibitory effect on EMT. The above result suggests that both affibody and affibody-based ADCs possess the targeted blockage of the carcinogenic process originating from virus.

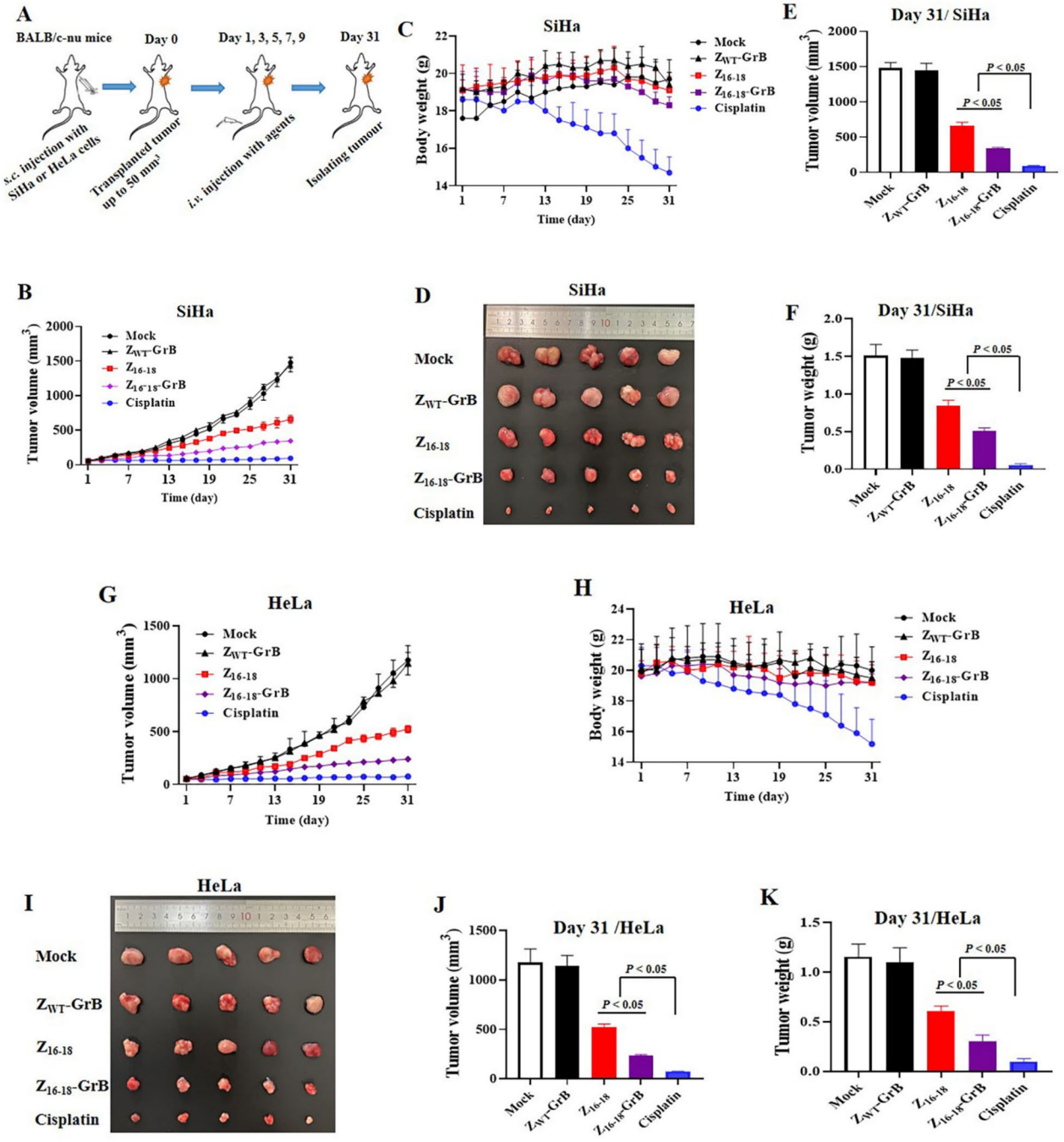

Fig. 7 Inhibition of tumor progression by bispecific affitoxin and affibody in vivo. **A** Sketch map of cell injection and agents administration into the nude mice. Subcutaneous injection of SiHa (1×10^7) or HeLa (1×10^7) cells; Intravenous injection of agents (0.1 nmol/g weight of $Z_{16\text{-}18}$-GrB, or $Z_{16\text{-}18}$, or Z_{WT}-GrB; Cisplatin (0.01 nmol/g weight) served as positive control). **B** Tumor growth curve in SiHa tumor-bearing mice. **C** Average body weight of SiHa tumor-bearing mice. **D** Tumor tissues separated on day 31 from SiHa tumor-bearing mice. **E** Average volume of tumors showed in **D**. **F** Average weight of tumors in **D**. **G** Tumor growth curve in HeLa tumor-bearing mice. **H** Average body weight of HeLa tumor-bearing mice. **I** Tumor tissues separated on day 31 from HeLa tumor-bearing mice. **J** Average volume of tumors showed in **I**. **K** Average weight of tumors showed in **I**. Data are presented as the mean ± SD (n = 5)

While ADCs show significant therapeutic effects, later stages of clinical treatment have revealed that immunogenicity or the use of heterologous toxins may lead some patients to produce neutralizing anti-drug antibodies (ADAs), which can diminish efficacy or cause adverse reactions [40, 41]. GrB, as the strongest one of granzymes, is an endogenous effector molecule released by immune effector cells, including cytotoxic T lymphocytes (CTLs) and natural killer (NK) cells, and it induces apoptosis in target cells via the perforin-granzyme pathway,

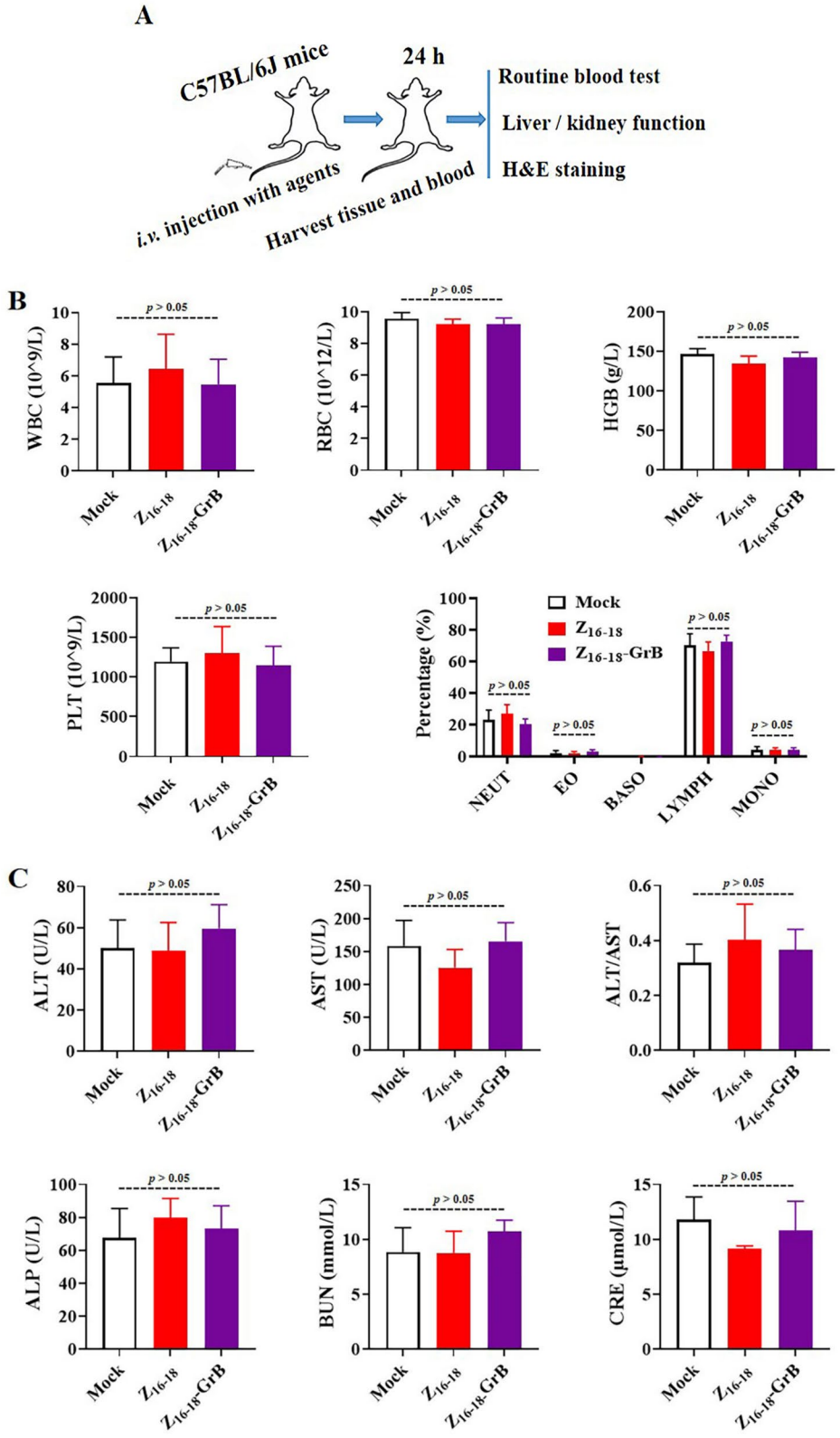

Fig. 8 No production of acute toxicity by bispecific affitoxin and affibody in vivo. **A** Sketch map of agents administration (0.1 nmol/g weight) and test plan. **B** Blood routine examination. WBC (white blood cells), RBC (red blood cells), PLT (platelets), HGB (hemoglobin), NEUT (neutrophils), EO (eosinophils), BASO (basophils), LYMPH (lymphocytes), MONO (monocytes). **C** Evaluation of liver and kidney function. Liver function indexes of ALT (glutamic-pyruvic transaminase), AST (glutamic- oxaloacetic transaminase), and ALP (alkaline phosphatase). Kidney function indexes of BUN (blood urea nitrogen) and CRE (creatinine). **D** H&E staining of liver and kidney tissue section. Data are presented as the mean ± SD (n = 5)

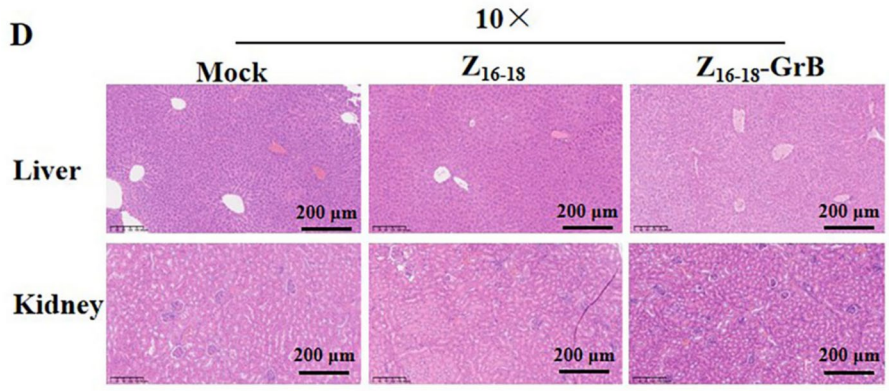

Fig. 8 (continued)

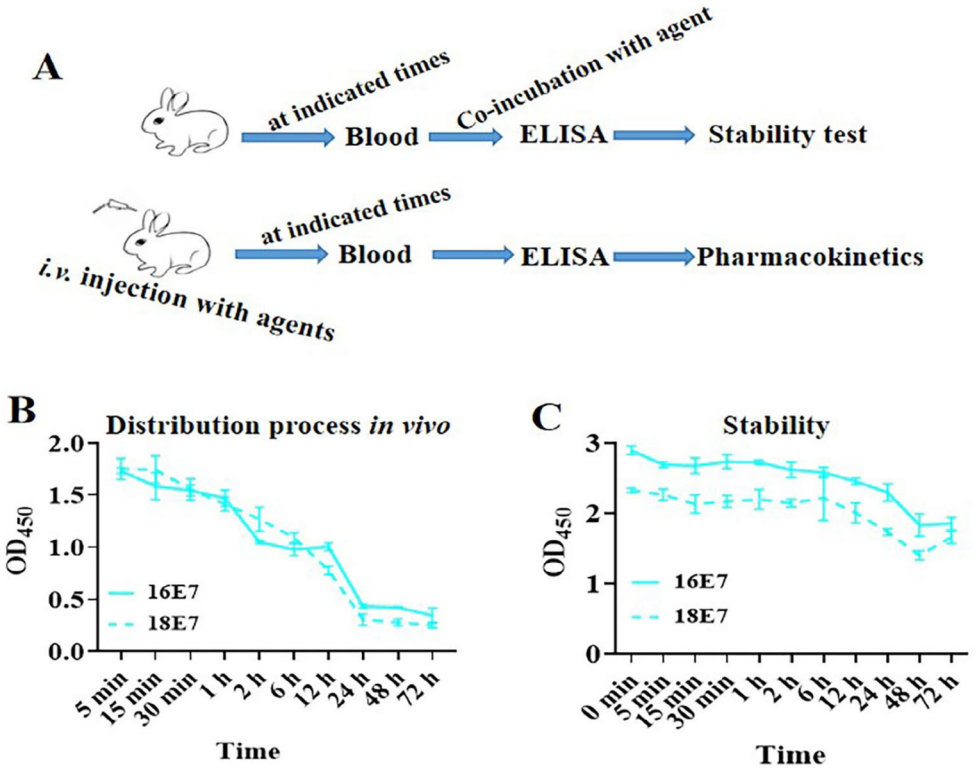

Fig. 9 Investigation of pharmacokinetics and stability of bispecific affitoxin. **A** Evaluation plan of pharmacokinetics and stability of bispecific affitoxin. **B** Pharmacokinetics detection of post-infusion bispecific affitoxin by ELISA. **C** Stability evaluation of co-incubated bispecific affitoxin with rabbit blood by ELISA. Full lines represent the HPV16 E7 protein as coated antigen in ELISA; Dotted lines represent the HPV18 E7 protein as coated antigen in ELISA. Data are presented as the mean ± SD (n = 3)

representing a key mechanism in anti-infection and anti-tumor responses [14]. The ADC agents of affibody fused with GrB developed in the present study could simultaneously interact with both target proteins of HPV16E7 and HPV18E7, as well as specifically bound to HPV16 + and HPV18 + CC cells and significantly induced apoptosis in these cells. While only affibody agent (without fusion with GrB) also induced notable apoptosis in HPV16 + and HPV18 + CC cells, the degree of apoptosis was less pronounced compared to the affitoxins, demonstrating the potential of affitoxin in anti-tumor therapy. In vivo anti-tumor experiments confirmed that the affitoxin exhibited stronger anti-tumor effects than affibody. After administration, the affitoxin didn't cause alterations in hematological parameters and liver/kidney function, and performed the advantages of application, such as: rapid distribution and specific enrichment in tumor tissue within 30 min after entering the bloodstream; especially, proteases-resistant in the plasma. The results suggested

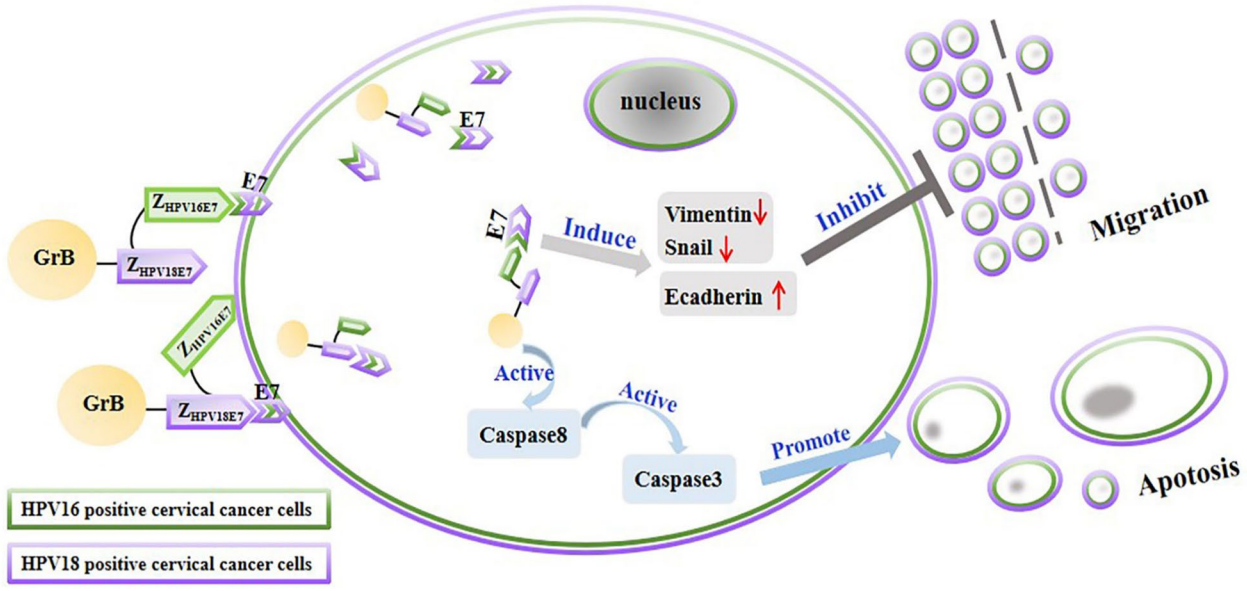

Fig. 10 Schematic representation of dual-function of bispecific affitoxins in HPV16 or 18 type-cervical cancer

the promising pharmacological potential for ADCs based on affibody.

Conclusion

In summary, this work has developed a bispecific affitoxin that simultaneously targets HPV16 and HPV18 type CC cells. Both in vitro and in vivo studies have validated its targeted binding, tumor growth and migration inhibition, induction of target cell apoptosis, absence of acute toxic reactions, and a certain degree of stability. ADCs based on affibody demonstrate a significant dual-functional advantage, combining the targeted inhibitory of the affibody with the cytotoxicity of the toxin molecule (Fig. 10). Our research offers a novel design and approach for targeted therapy in CC (cervical cancer).

Supplementary Information

The online version contains supplementary material available at https://doi.org/10.1186/s12967-025-06971-9.

Additional file1

Author contributions

Kairong Wan and Lijun Yu: Writing-original draft, Methodology, Formal analysis, Validation. Sicong Feng: Validation, Data analysis. Yanheng Li: Visualization, Methodology. Zhenyun Xie: Visualization, Writing revision. Xisha Jing and Junze Wu: Formal analysis. Lifang Zhang: Project administration, Conceptualization, Supervision. Wenshu Li: Conceptualization, Project administration, Writing-review & editing, Funding acquisition. All authors read and approved the final manuscript.

Funding

This study was supported by National Natural Science Foundation of China (No. 81973216) and the Basic Public Welfare Research Project of Zhejiang Province, China (LY23C010003).

Declarations

Conflict of interest

The authors declare no conflict of interest.

Ethical approval

This study is approved by the Medical Ethics Committee of Wenzhou Medical University, Wenzhou, Zhejiang, China. The experiments on animals were performed in accordance with the Helsinki Declaration.

Author details

[1]Department of Pathogen Biology and Immunology, School of Basic Medical Sciences, Wenzhou Medical University, Zhejiang 325032, China
[2]Communication Department, Technical University of Valencia, 46022 Valencia, Spain

Received: 3 May 2025 / Accepted: 4 August 2025
Published online: 22 September 2025

References

1. Singh D, Vignat J, Lorenzoni V, Eslahi M, Ginsburg O, Lauby-Secretan B, et al. Global estimates of incidence and mortality of cervical cancer in 2020: a baseline analysis of the WHO global cervical cancer elimination initiative. Lancet Glob Health. 2023;11(2):e197–206. https://doi.org/10.1016/S2214-109X(22)00501-0.
2. Perkins RB, Wentzensen N, Guido RS, Schiffman M. Cervical cancer screening: a review. JAMA. 2023;330(6):547–58. https://doi.org/10.1001/jama.2023.13174.
3. Simms KT, Keane A, Nguyen DTN, Caruana M, Hall MT, Lui G, Gauvreau C, et al. Benefits, harms and cost-effectiveness of cervical screening, triage and treatment strategies for women in the general population. Nat Med. 2023;29(12):3050–8. https://doi.org/10.1038/s41591-023-02600-4.
4. Pastan I, Willingham MC, FitzGerald DJ. Immunotoxins. Cell. 1986;47(5):641–8. https://doi.org/10.1016/0092-8674(86)90506-4.
5. Chau CH, Steeg PS, Figg WD. Antibody-drug conjugates for cancer. Lancet. 2019;394(10200):793–804. https://doi.org/10.1016/S0140-6736(19)31774-X.
6. Dumontet C, Reichert JM, Senter PD, Lambert JM, Beck A. Antibody-drug conjugates come of age in oncology. Nat Rev Drug Discov. 2023;22(8):641–61. https://doi.org/10.1038/s41573-023-00709-2.
7. Drago JZ, Modi S, Chandarlapaty S. Unlocking the potential of antibody-drug conjugates for cancer therapy. Nat Rev Clin Oncol. 2021;18(6):327–44. https://doi.org/10.1038/s41571-021-00470-8.

8. Cortés J, Kim SB, Chung WP, Im SA, Park YH, Hegg R, et al. Trastuzumab deruxtecan versus trastuzumab emtansine for breast cancer. N Engl J Med. 2022;386(12):1143–54. https://doi.org/10.1056/NEJMoa2115022.
9. Ansell SM, Radford J, Connors JM, Długosz-Danecka M, Kim WS, Gallamini A, et al. Overall survival with brentuximab vedotin in stage III or IV Hodgkin's lymphoma. N Engl J Med. 2022;387(4):310–20. https://doi.org/10.1056/NEJMoa2206125.
10. Advani RH, Moskowitz AJ, Bartlett NL, Vose JM, Ramchandren R, Feldman TA, et al. Brentuximab vedotin in combination with nivolumab in relapsed or refractory Hodgkin lymphoma: 3-year study results. Blood. 2021;138(6):427–38. https://doi.org/10.1182/blood.2020009178.
11. Hurvitz SA, Hegg R, Chung WP, Im SA, Jacot W, Ganju V, et al. Trastuzumab deruxtecan versus trastuzumab emtansine in patients with HER2-positive metastatic breast cancer: updated results from DESTINY-Breast03, a randomised, open-label, phase 3 trial. Lancet. 2023;401(10371):105–17. https://doi.org/10.1016/S0140-6736(22)02420-5.
12. Zhang Q, Zhu H, Cui Z, Li Y, Zhuo J, Ye J, et al. The HPV16E7 affibody as a novel potential therapeutic agent for treating cervical cancer is likely internalized through dynamin and caveolin-1 dependent endocytosis. Biomolecules. 2022;12(8):1114. https://doi.org/10.3390/biom12081114.
13. Sexton K, Tichauer K, Samkoe KS, Gunn J, Hoopes PJ, Pogue BW. Fluorescent affibody peptide penetration in glioma margin is superior to full antibody. PLoS ONE. 2013;8(4): e60390. https://doi.org/10.1371/journal.pone.0060390.
14. Vrazo AC, Hontz AE, Figueira SK, Butler BL, Ferrell JM, Binkowski BF, et al. Live cell evaluation of granzyme delivery and death receptor signaling in tumor cells targeted by human natural killer cells. Blood. 2015;126(8):e1–10. https://doi.org/10.1182/blood-2015-03-632273.
15. Aubert A, Lane M, Jung K, Granville DJ. Granzyme B as a therapeutic target: an update in 2022. Expert Opin Ther Targets. 2022;26(11):979–93. https://doi.org/10.1080/14728222.2022.2161890.
16. Li Z, Ma R, Tang H, Guo J, Shah Z, Zhang J, et al. Therapeutic application of human type 2 innate lymphoid cells via induction of granzyme B-mediated tumor cell death. Cell. 2024;187(3):624-641.e23. https://doi.org/10.1016/j.cell.2023.12.015.
17. Hoppe-Seyler K, Bossler F, Braun JA, Herrmann AL, Hoppe-Seyler F. The HPV E6/E7 oncogenes: key factors for viral carcinogenesis and therapeutic targets. Trends Microbiol. 2018;26(2):158–68. https://doi.org/10.1016/j.tim.2017.07.007.
18. Szymonowicz KA, Chen J. Biological and clinical aspects of HPV-related cancers. Cancer Biol Med. 2020;17(4):864–78. https://doi.org/10.20892/j.issn.2095-3941.2020.0370.
19. Bortnik V, Wu M, Julcher B, Salinas A, Nikolic I, Simpson KJ, et al. Loss of HPV type 16 E7 restores cGAS-STING responses in human papilloma virus-positive oropharyngeal squamous cell carcinomas cells. J Microbiol Immunol Infect. 2021;54(4):733–9. https://doi.org/10.1016/j.jmii.2020.07.010.
20. Liu H, Xu J, Yang Y, Wang X, Wu E, Majerciak V, et al. Oncogenic HPV promotes the expression of the long noncoding RNA lnc-FANCI-2 through E7 and YY1. Proc Natl Acad Sci U S A. 2021;118(3): e2014195118. https://doi.org/10.1073/pnas.2014195118.
21. Antonioli M, Pagni B, Vescovo T, Ellis R, Cosway B, Rollo F, Bordoni V, et al. HPV sensitizes OPSCC cells to cisplatin-induced apoptosis by inhibiting autophagy through E7-mediated degradation of AMBRA1. Autophagy. 2021;17(10):2842–55. https://doi.org/10.1080/15548627.2020.1847444.
22. Galliverti G, Tichet M, Domingos-Pereira S, Hauert S, Nardelli-Haefliger D, Swartz MA, et al. Nanoparticle conjugation of human papillomavirus 16 E7-long peptides enhances therapeutic vaccine efficacy against solid tumors in mice. Cancer Immunol Res. 2018;6(11):1301–13. https://doi.org/10.1158/2326-6066.CIR-18-0166.
23. Smalley Rumfield C, Pellom ST, Morillon Ii YM, Schlom J, Jochems C. Immunomodulation to enhance the efficacy of an HPV therapeutic vaccine. J Immunother Cancer. 2020;8(1): e000612. https://doi.org/10.1136/jitc-2020-000612.
24. Huang B, Zhou Z, Liu J, Wu X, Li X, He Q, et al. The role of monoamine oxidase A in HPV-16 E7-induced epithelial-mesenchymal transition and HIF-1α protein accumulation in non-small cell lung cancer cells. Int J Biol Sci. 2020;16(14):2692–703. https://doi.org/10.7150/ijbs.46966.
25. Wang A, Zhou D, Krawczyk E, Li T, Simic V, Lu J, et al. Overexpression of the telomerase holoenzyme induces EMT and tumorigenesis of HPV-immortalized keratinocytes. J Med Virol. 2023;95(4): e28681. https://doi.org/10.1002/jmv.28681.
26. Zhou Z, Wu X, Zhan R, Li X, Cheng D, Chen L, et al. Exosomal epidermal growth factor receptor is involved in HPV-16 E7-induced epithelial-mesenchymal transition of non-small cell lung cancer cells: a driver of signaling in vivo. Cancer Biol Ther. 2022;23(1):1–13. https://doi.org/10.1080/15384047.2022.2133332.
27. Matarrese P, Vona R, Ascione B, Paggi MG, Mileo AM. Physical interaction between HPV16E7 and the actin-binding protein gelsolin regulates epithelial-mesenchymal transition via HIPPO-YAP axis. Cancers. 2021;13(2):353. https://doi.org/10.3390/cancers13020353.
28. Trimble CL, Peng S, Kos F, Gravitt P, Viscidi R, Sugar E, et al. A phase I trial of a human papillomavirus DNA vaccine for HPV16+ cervical intraepithelial neoplasia 2/3. Clin Cancer Res. 2009;15(1):361–7. https://doi.org/10.1158/1078-0432.CCR-08-1725.
29. Trimble CL, Morrow MP, Kraynyak KA, Shen X, Dallas M, Yan J, Edwards L, et al. Safety, efficacy, and immunogenicity of VGX-3100, a therapeutic synthetic DNA vaccine targeting human papillomavirus 16 and 18 E6 and E7 proteins for cervical intraepithelial neoplasia 2/3: a randomised, double-blind, placebo-controlled phase 2b trial. Lancet. 2015;386(10008):2078–88. https://doi.org/10.1016/S0140-6736(15)00239-1.
30. Khalil MI, Yang C, Vu L, Chadha S, Nabors H, James CD, et al. The membrane-associated ubiquitin ligase MARCHF8 stabilizes the human papillomavirus oncoprotein E7 by degrading CUL1 and UBE2L3 in head and neck cancer. J Virol. 2024;98(2): e0172623. https://doi.org/10.1128/jvi.01726-23.
31. Zhu J, Kamara S, Wang Q, Guo Y, Li Q, Wang L, et al. Novel affibody molecules targeting the HPV16 E6 oncoprotein inhibited the proliferation of cervical cancer cells. Front Cell Dev Biol. 2021;9: 677867. https://doi.org/10.3389/fcell.2021.677867.
32. Xue X, Wang B, Du W, Zhang C, Song Y, Cai Y, et al. Generation of affibody molecules specific for HPV16 E7 recognition. Oncotarget. 2016;7(45):73995–4005. https://doi.org/10.18632/oncotarget.12174.
33. Jiang P, Wang L, Hou B, Zhu J, Zhou M, Jiang J, et al. A novel HPV16 E7-affitoxin for targeted therapy of HPV16-induced human cervical cancer. Theranostics. 2018;8(13):3544–58. https://doi.org/10.7150/thno.24607.
34. Wang W, Tan X, Jiang J, Cai Y, Feng F, Zhang L, et al. Targeted biological effect of an affitoxin composed of an HPV16E7 affibody fused with granzyme B (ZHPV16E7-GrB) against cervical cancer in vitro and in vivo. Curr Cancer Drug Targets. 2020. https://doi.org/10.2174/1568009620666201207145720.
35. Khirehgesh MR, Sharifi J, Safari F, Akbari B. Immunotoxins and nanobody-based immunotoxins: review and update. J Drug Target. 2021;29(8):848–62. https://doi.org/10.1080/1061186X.2021.1894435.
36. Van Tine BA, Hubbard JM, Mita MM, Barve MA, Hamilton EP, Brenner AJ, et al. A phase 1 study of the novel immunotoxin MT-5111 in patients with HER2+ tumors: interim results. J Clin Oncol. 2022;40(16_suppl):2583–2583. https://doi.org/10.1200/JCO.2022.40.16_suppl.2583.
37. Dhillon S. Moxetumomab pasudotox: first global approval. Drugs. 2018;78(16):1763–7. https://doi.org/10.1007/s40265-018-1000-9.
38. Markham A. Tisotumab vedotin: first approval. Drugs. 2021;81(18):2141–7. https://doi.org/10.1007/s40265-021-01633-8.
39. Monk BJ, Enomoto T, Kast WM, McCormack M, Tan DSP, Wu X, et al. Integration of immunotherapy into treatment of cervical cancer: recent data and ongoing trials. Cancer Treat Rev. 2022;106: 102385. https://doi.org/10.1016/j.ctrv.2022.102385.
40. de Spéville BD, Moreno V. Antidrug antibodies and drug development: challenges in the immunotherapy era. Clin Cancer Res. 2021;27(10):2669–71. https://doi.org/10.1158/1078-0432.CCR-21-0168.
41. Garcês S, Demengeot J. The immunogenicity of biologic therapies. Curr Probl Dermatol. 2018;53:37–48. https://doi.org/10.1159/000478077.

Publisher's Note